Effect of Eu3+ and Tb3+ ions concentration on the mechanical, structural, and photoluminescence properties of phosphate glass fibers

Rachid Mahiou, Oumaima Jamal Eddine, Damien Boyer, Mehdi El Bouchti, Aicha Boukhriss, Omar Cherkaoui, Hassan Hannache, Said Gmouh

Optical Materials 122 (2021) 111664

Contents lists available at ScienceDirect

Optical Materials

journal homepage: www.elsevier.com/locate/optmat

Research Article

Effect of Eu^{3+} and Tb^{3+} ions concentration on the mechanical, structural, and photoluminescence properties of phosphate glass fibers

Oumaima Jamal Eddine [a], Damien Boyer [b], Mehdi El Bouchti [c], Aicha Boukhriss [c], Omar Cherkaoui [c], Rachid Mahiou [b], Hassan Hannache [a,d], Said Gmouh [a,*]

[a] Hassan II University of Casablanca, Faculty of Sciences Ben M'scik, Chemistry Department, Laboratory LIMAT, Avenue Driss El Harti, BP 7955, Casablanca, Morocco
[b] Université Clermont Auvergne, Clermont Auvergne INP, CNRS, ICCF, F-63000, Clermont-Ferrand, France
[c] Higher School of Textile and Clothing Industries, Laboratory REMTEX, km 8, Route d'El Jadida, BP 7731, Oulfa, Casablanca, Morocco
[d] Mohammed VI Polytechnic University, Materials Science and Nanoengineering Department, Lot 660, Hay Moulay Rachid, Benguerir, Morocco

ARTICLE INFO

Keywords:
Phosphate glass fibers
Eu^{3+}
Tb^{3+}
Mechanical properties
Photoluminescence

ABSTRACT

Two series of phosphate glasses belonging to the (65-x) P_2O_5–35CaO–xRE_2O_3 system (RE = Eu or Tb; $0 \leq x \leq 6$ mol%) were prepared by the melt-quenching technique. All compositions were successfully drawn as continuous monofilaments fibers. The effect of Eu^{3+} and Tb^{3+} ions concentration on their mechanical, structural, and photoluminescence properties was investigated. The results revealed that the highest tensile strength was 1031 ± 34 MPa for fibers doped with 6 mol% of Eu_2O_3 and 1014 ± 65 MPa for fibers doped with 6 mol% of Tb_2O_3. The addition of RE_2O_3 showed an increase in density and Tg. A structural investigation was carried out using FTIR spectroscopy. The photoluminescence properties in terms of excitation and emission spectra were investigated in detail. The most intense emission band at 611 nm corresponds to the $^5D_0 \rightarrow {}^7F_2$ transition of Eu^{3+} ions under 392 nm excitation was observed for fibers doped with 6 mol% of Eu_2O_3. The most intense emission band at 543 nm corresponds to the $^5D_4 \rightarrow {}^7F_5$ transition of Tb^{3+} ions under 374 nm excitation was observed for fibers doped with 6 mol% of Tb_2O_3. These two compositions exhibited the highest absolute quantum yield, reaching 20.25% and 4.81%, respectively.

1. Introduction

Phosphate glasses (PGs) are easy to produce and have great advantages due to their special properties that include high UV transparency, low infrared transparency, low melting temperature point, high thermal expansion, low dispersion, and regarded as better hosts for lanthanide ions (Ln^{3+}) [1–3]. It is well known that the luminescence properties of rare-earth ions (RE ions) result from their electronic structure [Xe] $4f^n5d^26s^1$. When these ions are inserted into a glassy network, the most stable and predominant oxidation state is trivalent and the 5d and 6s electronic layers are empty [4]. Among these different ions, Eu^{3+} ([Xe] $4f^6$) and Tb^{3+} ([Xe] $4f^8$) ions have been widely used as fluorescence-generating ions for the development of many luminescent materials, including PGs and phosphate glass fibers (PGFs) [5–7].

Generally, PGs doped with RE ions are well known for their high optical quality, as well as their higher doping concentration in comparison with that observed in silicate and borate glasses. In particular, PGs doped with Eu^{3+} and Tb^{3+} have been widely used in various optical devices such as optical fibers, amplifiers and lasers [7–9]. Their luminescence spectra are composed of many narrow lines as a consequence of 4f–4f transitions which are slightly sensitive to the environment of the RE^{3+} ion due to the shielding effect of $4f^6$ electrons by 5s and 5p electrons in outer shells in the RE^{3+} [4,10,11]. They also present a sharp and bright red (at around 600–620 nm) and green (at around 545 nm) emission, respectively, which are hypersensitive to the RE^{3+} ion surroundings than normal f–f transitions [12,13].

In the past several decades, the optical properties and the mechanisms of various vitreous systems based on calcium phosphate P_2O_5–CaO doped with europium or terbium ions have been studied [14–19]. Attention has been drawn to understand the basic theoretical models and experimental studies of the energy level structure, decay times of the excited states, energy transfer mechanisms, site symmetry

* Corresponding author.
E-mail addresses: jamaleddine.oumaima@gmail.com (O. Jamal Eddine), damien.boyer@sigma-clermont.fr (D. Boyer), melbouchti@gmail.com (M. El Bouchti), aicha.boukhriss@gmail.com (A. Boukhriss), omarcherkaoui61@gmail.com (O. Cherkaoui), rachid.mahiou@uca.fr (R. Mahiou), hassan.hannache@gmail.com (H. Hannache), s.gmouh1@gmail.com (S. Gmouh).

https://doi.org/10.1016/j.optmat.2021.111664
Received 15 August 2021; Accepted 4 October 2021

determination, anomalous spectral properties, etc. However, to the best of our knowledge, studies of the effect of the percentage of Eu_2O_3 and Tb_2O_3 in the P_2O_5–CaO system on the structural and photoluminescence properties were not mentioned. In this regard, new PGs with compositions based on the P_2O_5–CaO–RE_2O_3 system with RE = Eu or Tb were prepared. On the other hand, the elaborated PGs were stretched into PGFs to demonstrate the possibility of functionalizing small diameter non-woven PGFs (average diameter of a few micrometers) by doping with RE ions. It is expected that the introduction of the europium or terbium oxides into the studied glassy systems may affect the mechanical, structural and photoluminescence properties of the investigated fibers.

2. Experiment

Two series of PGs doped with RE ions were prepared by the conventional melt-quenching technique. Series 1 presents PGs doped with europium ions (see Table 1) and belongs to the (65-x) P_2O_5–35CaO–xEu_2O_3 system while series 2 presents PGs doped with terbium ions (see Table 2) and belongs to the (65-x) P_2O_5–35CaO–xTb_2O_3 system, where $0 \leq x \leq 6$ mol%. The binary glass (OJ_0) without the addition of RE_2O_3 was prepared in order to estimate the influence of the latter on the properties of PGFs. The starting materials used are high-purity commercial reagents (Sigma-Aldrich): tricalcium phosphate $Ca_3(PO_4)_3$ (≥96.0%), europium oxide Eu_2O_3 (≥99.99%), and terbium oxide Tb_2O_3 (≥99.99%). Afterward, the materials were mixed homogeneously and then heated to 600 °C for 2 h in a platinum crucible. Subsequently, it was melted at 900 °C for 1 h and cooled in air.

All PGs samples were successfully transformed into continuous monofilaments fibers by a melt-draw spinning process. The spinning process reported here was carried out with the steps and precautions described in detail in our previous papers [20,21]. In this study, the winding speed was set at 538 rpm and the optimal spinning temperatures are 750 °C (temperature at the top) and 550 °C (temperature at the bottom). The average diameter measured for several PGFs was 22.1 ± 0.8 μm. No correlation was noticed with the composition and diameters values obtained. All PGFs samples are colorless and transparent under daylight. Fig. 1 shows photographs of some PGs and PGFs samples of the compositions: OJ_0 (under daylight), and OJ_7, OJ_{11} and OJ_{14} (under UV-A light illumination; $\lambda_{excitation}$ = 365 nm). Under the UV-A lamp, Eu^{3+}-doped samples show a strong red fluorescence, while Tb^{3+}-doped samples show a bright green fluorescence, observed with the naked eye. However, under the same preparation conditions, the PGFs doped with more than 6 mol% of RE_2O_3 showed low fluorescence under the UV-A lamp compared to the other PGFs compositions.

Scanning electron microscope (SEM) image of the OJ_6 fiberglass sample was taken with ZEISS Supra 55VP scanning electron microscope. The mechanical properties of the PGFs were investigated by tensile tests using a tensile testing machine (model LUDWIC Mpk, made in Germany) [20,21], according to BS ISO 11566:1996 [22]. The values of the density (ρ) were measured by immersing the samples of PGFs according to the Archimedes technique (BS 10119) [21]. Then, the molar volume values (V_m) were calculated using the expression $V_m = M/\rho$, where M is the molecular weight of PGFs. Differential thermal analysis (DTA) was performed using a PerkinElmer DTA7 instrument under a flowing nitrogen atmosphere with a fixed heating rate of 10 °C/min up to a maximum temperature of 1000 °C. Errors in measurement are ±2 °C. The X-ray diffraction (XRD) measurements were carried out using a Siemens D501 diffractometer (λ_{Cu} = 1.5406 Å) in the range of 10–80°. The Fourier transform infrared (FTIR) spectra were recorded at room temperature within the wavenumber range 400–4000 cm^{-1} using a Thermo Electron spectrometer (Nicolet 5700-FTIR model). Photoluminescence (PL) spectra of doped PGFs samples were recorded using as excitation source a xenon lamp monochromatized through a TRIAX 180 Jobin-Yvon/Horiba and TRIAX 550 Jobin-Yvon/Horiba monochromator equipped with R928 Hamamatsu photomultiplier as a detector. For the Eu^{3+}-doped PGFs samples (λ_{ex} = 392 nm) and the Tb^{3+}-doped PGFs samples (λ_{ex} = 374 nm), the PL data were recorded in the range 400–750 nm. Quantum yield (QY) efficiencies were measured using the Hamamatsu Photonics measurement system under the reference C9920-02G. The setup comprises a 150 W monochromatized Xe lamp, an integrating sphere (Spectralon Coating, Ø = 3.3 in.), and a high sensitivity CCD spectrometer for detecting the whole spectral luminescence simultaneously. The absolute quantum yield (Φa) in percent was calculated using the expression $\Phi a = \Phi i^* Abs^* 100\%$, where Φi is the internal quantum yield (the ratio between the emitted and the absorbed photons by the material upon external excitation) and *Abs* is the Absorbance. The CIE (Commission Internationale de l'Éclairage, International Commission on Illumination) color coordinates (x,y) were measured in an integrating sphere with a diode array rapid analyzer system (GL Optic integrating sphere GLS 500). All luminescence experiments were performed at ambient air.

Table 1
Nominal composition (mol%), calculated (O/P) ratio, density (ρ), and molar volume (*Vm*) of Eu^{3+}-doped PGFs.

Series 1	Compounds (in mol%)			O/P	ρ [g.cm^{-3}]	V_m [cm^3.mol^{-1}]
	P_2O_5	CaO	Eu_2O_3			
OJ_0	65	35	0	2.61	2.18	51.33
OJ_1	64.5	35	0.5	2.64	2.42	46.67
OJ_2	64	35	1	2.67	2.47	46.15
OJ_3	63	35	2	2.73	2.56	45.35
OJ_4	62	35	3	2.79	2.65	44.60
OJ_5	61	35	4	2.86	2.78	43.27
OJ_6	60	35	5	2.93	2.94	41.63
OJ_7	59	35	6	3.00	3.04	40.95

Table 2
Nominal composition (mol%), calculated (O/P) ratio, density (ρ), and molar volume (*Vm*) of Tb^{3+}-doped PGFs.

Series 2	Compounds (in mol%)			O/P	ρ [g.cm^{-3}]	V_m [cm^3.mol^{-1}]
	P_2O_5	CaO	Tb_2O_3			
OJ_0	65	35	0	2.61	2.18	51.33
OJ_8	64.5	35	0.5	2.64	2.47	45.75
OJ_9	64	35	1	2.67	2.51	45.47
OJ_{10}	63	35	2	2.73	2.63	44.25
OJ_{11}	62	35	3	2.80	2.71	43.77
OJ_{12}	61	35	4	2.87	2.85	42.40
OJ_{13}	60	35	5	2.94	3.01	40.89
OJ_{14}	59	35	6	3.01	3.09	40.56

3. Results and discussion

3.1. Morphology

SEM analysis was used to observe the appearance of PGFs surface. Fig. 2 shows a SEM image at 800 times magnification of OJ_6 sample belonging to the $60P_2O_5$–35CaO–$5Eu_2O_3$ system. As it can be seen from this figure, the OJ_6 PGF appears smooth and homogeneous.

3.2. Mechanical properties

The results of the tensile tests on OJ_0, OJ_7, OJ_{11}, and OJ_{14} samples are presented in Table 3. The values of tensile strength (σ), Young's modulus (*E*) and breaking strain (ε) of the reference PGFs of $65P_2O_5$–35CaO system were 724 ± 53 MPa, 63 ± 3 GPa, and 1.16 ± 0.10%, respectively. Slivka et al. [23] tested individual calcium PGFs of the $66P_2O_5$–23CaO–8ZnO–$3Fe_2O_3$ system with a diameter of 25.5 μm. They found that the values obtained of tensile strength, Young's modulus, and breaking strain were 513 MPa, 43 GPa, and 1.3%, respectively. The significant values of mechanical quantities found in

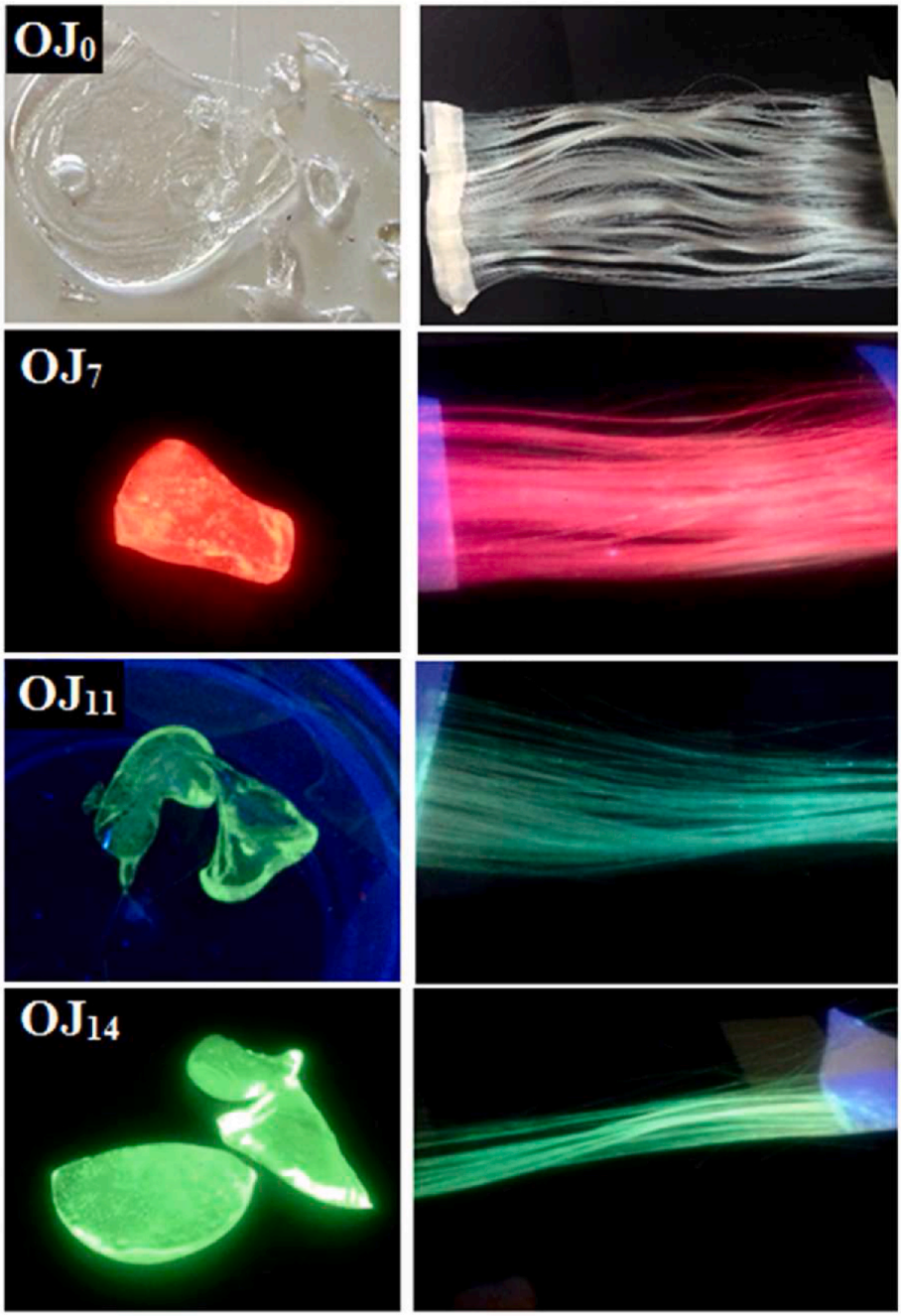

Fig. 1. Photographs of some PGs and PGFs; OJ_0 (under daylight); OJ_7, OJ_{11}, and OJ_{14} (under UV-A light illumination; $\lambda_{excitation} = 365$ nm).

our study can be explained by the dependence of the diameter on the tensile strength, and therefore on the breaking strain and Young's modulus. On the other hand, Ahmed et al. [24] tested individual calcium phosphate glass fibers of the $50P_2O_5$–50CaO system with a diameter of 20 μm. They found that the values obtained of tensile strength and Young's modulus were 475 MPa and 44 GPa, respectively. These values are significantly lower than the values obtained in our study. This result can be explained by the excessive amount of CaO compared to P_2O_5, which influenced the mechanical properties of PGFs. Besides the effect of diameter and composition, a number of studies have shown that the spinning temperature plays a key role in the mechanical performance of fiberglass [25].

A significant increase in tensile strength, Young's modulus and thus breaking strain of fibers doped with RE_2O_3 compared to the reference PGFs (OJ_0) is observed. The tensile strength values obtained were 1031 ± 34 MPa for fibers doped with 6 mol% of Eu_2O_3, and 861 ± 71 MPa and 1014 ± 65 MPa for fibers doped with 3 and 6 mol% of Tb_2O_3, respectively. The Young's modulus values obtained for these 3 compositions were 80 ± 6 GPa, 73 ± 4 GPa, and 79 ± 7 GPa, respectively. At last, the values of breaking strain for these compositions are 1.29 ± 0.23%, 1.18 ± 0.11%, and 1.28 ± 0.20%, respectively. The evolution of the mechanical properties of these fibers is due to the addition of RE_2O_3 with an appropriate amount in the PG composition. In addition, it has been suggested that fibers with a high modulus are more rigid.

3.3. Density and molar volume

Tables 1 and 2 present the O/P ratio values and the average values of

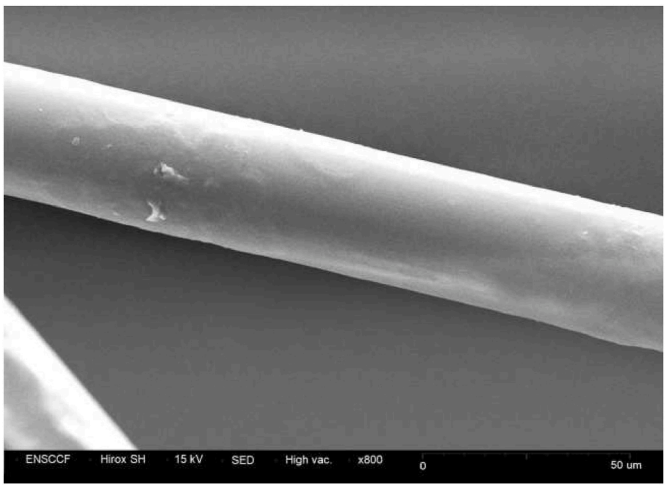

Fig. 2. SEM image of OJ_6 Eu^{3+}-doped PGF.

density measurements and molar volume for all studied PGFs compositions. Fig. 3 shows the evolution of ρ and V_m as a function of each composition, from series 1 (see Fig. 3 (a)) and series 2 (see Fig. 3 (b)).

As shown in Tables 1 and 2, O/P = 2.61 for the reference PGFs (OJ_0), which means that the ultraphosphate groups ($5/2 < O/P < 3$) of a long phosphate chain (Q^3) are dominant. These groups are highly concentrated in P_2O_5 of which the arrangement of PO_4 tetrahedra forms a three-dimensional network. When these fibers are doped with 6 mol% of Eu_2O_3 or Tb_2O_3, the molar ratio O/P becomes equal to 3, which characterizes the metaphosphate groups rich in PO_4^{3-} (Q^2). These groups present a network formed of long chains and rings. Indeed, when the Eu_2O_3 or Tb_2O_3 content increases, it can be noted that the content of (Q^3) structural entities decreases, and thus the content of (Q^2) structural entities increases. Therefore, the bond length and bond angle of P–O–P in the glassy network structure also change [5].

Fig. 3 shows a linear increase in density as the RE_2O_3 content increases in the studied glassy systems. They increased from 2.18 g cm^{-3} for the OJ_0 PGFs to 3.04 g cm^{-3} for the OJ_7 PGFs and to 3.09 g cm^{-3} for the OJ_{14} PGFs. This increase can be explained by the fact that the molecular weights of Eu_2O_3 and Tb_2O_3 are greater than that of P_2O_5 and CaO and that the Eu^{3+} and Tb^{3+} ions have a strong aggregation. Furthermore, the molar volume of PGFs decreases with the RE_2O_3 content. These results indicate that the glassy network becomes more compact.

3.4. Thermal analysis

Fig. 4 shows the DTA curves of OJ_0, OJ_7, OJ_{11}, and OJ_{14} PGFs. The values of glass transition temperature (Tg) and melting temperature (Tm) are collected in Table 3. The results show an increase in Tg and Tm values with the increase of RE_2O_3 content for both series. This increase is explained by the occupation of Eu^{3+} and Tb^{3+} ions of the interstitial sites of the glassy network. Therefore, the latter becomes more compact.

3.5. Structural characterization

The amorphous behavior of Eu^{3+} and Tb^{3+}-doped PGFs was confirmed for all compositions by XRD analysis. Fig. 5 shows 4 examples of XRD patterns of PGFs samples (OJ_0, OJ_7, OJ_{11}, and OJ_{14}). The broad hump characteristic in all XRD spectra indicates a non-crystalline structure in the glassy system.

Fig. 6 shows the infrared spectra of different samples from series 1 (Fig. 6a) and series 2 (Fig. 6b). As can be seen, the spectra of the fibers doped with RE_2O_3 show no significant changes. The FTIR spectrum of OJ_0 fibers shows seven dominant bands observed at 1231, 1184, 1103, 996, 915, 741, and 514 cm^{-1} within the wavenumber range 400–4000 cm^{-1}. The infrared band assignments of the PGFs are listed in Table 4.

The vibrational bands around 1231 and 1184 cm^{-1} are attributed to asymmetric $\upsilon_{as}(PO_2)$ and symmetric $\upsilon_s(PO_2)$ stretching, respectively [1, 26,27]. In this case, the two non-bridging oxygen (NBO) atoms easily connect to a phosphorus atom in the chain metaphosphate (Q^2). The absorption bands shown at 1103 and 996 cm^{-1} correspond to the asymmetric $\upsilon_{as}(PO_3)$ and symmetric $\upsilon_s(PO_3)$ stretching vibrations due to PO_4 tetrahedra containing 2 and 3 NBO atoms, respectively [1,28,29].

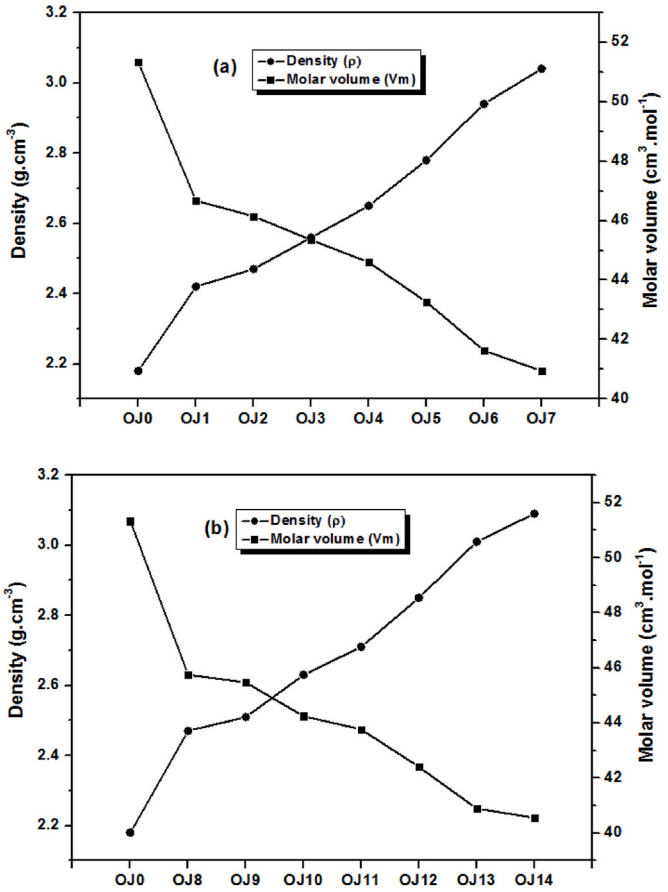

Fig. 3. Evolution of density (ρ) and molar volume (V_m) of **(a)** Eu^{3+}-doped PGFs compositions and **(b)** Tb^{3+}-doped PGFs compositions.

Table 3
Results of tensile tests and DTA analysis of PGFs samples.

PGFs code	Glass system	Tensile strength	Young's modulus	Breaking strain	Glass transition temperature	Melting temperature
		σ (MPa)	E (GPa)	ε (%)	Tg (°C)	Tm (°C)
OJ_0	$65P_2O_5$–35CaO	724 ± 53	63 ± 3	1.16 ± 0.10	370	769
OJ_7	$59P_2O_5$–35CaO–$6Eu_2O_3$	1031 ± 34	80 ± 6	1.29 ± 0.23	509	801
OJ_{11}	$62P_2O_5$–35CaO–$3Tb_2O_3$	861 ± 71	73 ± 4	1.18 ± 0.11	445	811
OJ_{14}	$59P_2O_5$–35CaO–$6Tb_2O_3$	1014 ± 65	79 ± 7	1.28 ± 0.20	513	833

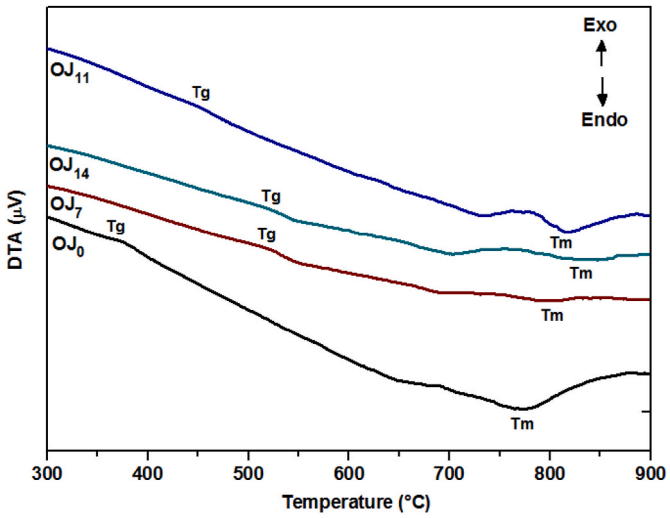

Fig. 4. DTA curves of PGFs samples at a heating rate of 10 °C/min under nitrogen atmosphere.

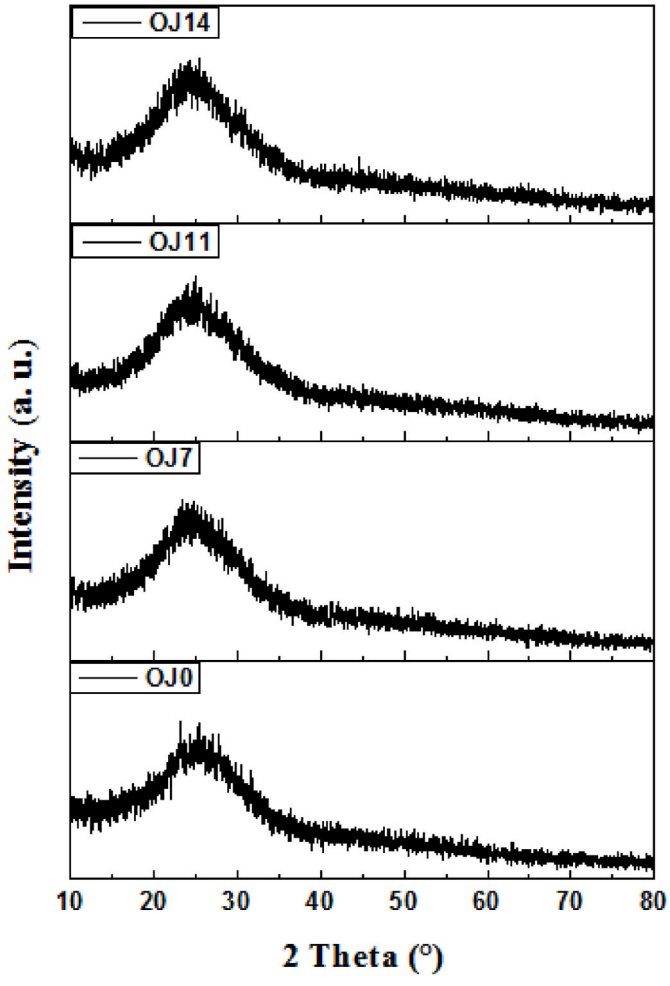

Fig. 5. X-ray diffraction patterns of PGFs samples.

These two bands are characteristic of the chain end groups (Q^1).

The vibrational bands centered at 915 and 741 cm^{-1} are attributed to the asymmetric υ_{as}(P—O—P) and symmetric υ_s(P—O—P) stretching vibrations, respectively, of the bridging oxygen (BO) atoms bonded to a phosphorus atom in a phosphate tetrahedron [5,30,31]. These two bands are characteristic of intermediate entities (Q^2).

At last, the broadband around 541 cm^{-1} can be ascribed to the deformation mode $\delta(PO_4)^{3-}$ of the isolated tetrahedra groups characteristic of phosphate units (Q^0) [20,32,33].

3.6. Photoluminescence properties

Fig. 7 shows the excitation spectra (PLE) recorded at room temperature for Eu^{3+}-doped fibers (Fig. 7 (a)) and Tb^{3+}-doped fibers (Fig. 7 (b)). The characteristic excitation transitions of Eu^{3+}-doped PGFs are $^7F_0 \rightarrow {}^5H_{3\text{-}7}$ (323 nm), $^7F_0 \rightarrow {}^5D_4$ (364 nm), $^7F_0 \rightarrow {}^5G_3$ (373 nm), $^7F_0 \rightarrow {}^5G_2$ (385 nm), $^7F_0 \rightarrow {}^5L_6$ (392 nm), $^7F_0 \rightarrow {}^5D_3$ (415 nm), and $^7F_0 \rightarrow {}^5D_2$ (486 nm). The most significant excitation transitions characteristic of Tb^{3+}-doped PGFs are $^7F_6 \rightarrow {}^5H_6$ (301 nm), $^7F_6 \rightarrow {}^5H_7$ (318 nm), $^7F_6 \rightarrow ({}^5G_2, {}^5L_8)$ (345 and 349 nm), $^7F_6 \rightarrow ({}^5G_4, {}^5L_9)$ (351 nm), $^7F_6 \rightarrow {}^5G_5$ (358 nm), $^7F_6 \rightarrow {}^5L_{10}$ (366 nm), $^7F_6 \rightarrow ({}^5G_6, {}^5D_3)$ (374 nm), and $^7F_6 \rightarrow {}^5D_4$ (384 nm). From the PLE spectra, the maximum excitation wavelengths obtained are 392 nm and 374 nm for Eu^{3+}-doped fibers and Tb^{3+}-doped fibers, respectively, which are therefore chosen to record the emission spectra (PL). Figs. 8 and 9 show the PL spectra recorded at room temperature for some Eu^{3+}-doped and Tb^{3+}-doped PGFs compositions, respectively, with different dopant concentrations. The inhomogeneous broadening of the lines in the excitation and emission spectra is due to differences in the local environments around the RE ions in the disordered glassy system that arise from variations in both the RE—O distances and in the coordination numbers of these elements [16,34,35].

Excitation energy is transferred nonradiatively to the $^5D_0$ state due to the relatively small energy gaps between the $^5D_1$, $^5D_2$, and $^5D_3$ states from which radiative transitions occur [36]. Therefore, all emission bands recorded under excitation at 392 nm are associated with $^5D_0 \rightarrow {}^7F_J$ (J = 0–4) transitions appearing in the range between 570 and 750 nm. These intense bands belonging to the internal 4f–4f transitions of Eu^{3+} ions appear in each spectrum. The characteristic emission bands of Eu^{3+}-doped PGFs located around 578, 592, 611, 651, and 697 nm correspond to the emission transitions $^5D_0 \rightarrow {}^7F_0$, $^5D_0 \rightarrow {}^7F_1$, $^5D_0 \rightarrow {}^7F_2$, $^5D_0 \rightarrow {}^7F_3$, and $^5D_0 \rightarrow {}^7F_4$, respectively.

In this study, we examine in detail the spectral distribution for each emission transition of Eu^{3+} ions in the (65-x) P_2O_5–35CaO–xEu system (with x = 2, 3, 5, and 6 mol%). Although the $^5D_0 \rightarrow {}^7F_0$ transition is often observed in emission spectra, it is strictly forbidden according to the standard Judd-Ofelt (JO) theory [12,37]. Previous studies indicate that the appearance of this transition can be attributed to J-mixing effects [38,39] or the mixing of low charge-transfer states in the wave functions of the $4f^6$ configuration [12,40]. This very weak transition is identified as an electric dipole (ED). The $^5D_0 \rightarrow {}^7F_1$ transition is an allowed magnetic dipole (MD) and its intensity is generally independent of the local symmetry [41–43]. The most intense band with red emission at 611 nm corresponds to the $^5D_0 \rightarrow {}^7F_2$ transition is hypersensitive to the local symmetry of Eu^{3+} ions [12,40]. This transition has a purely (ED) character. The $^5D_0 \rightarrow {}^7F_3$ transition is weak because it is forbidden according to the standard (JO) theory [5]. This transition is identified as (ED) character and can only gain intensity by J-mixing [44]. At last, the $^5D_0 \rightarrow {}^7F_4$ (ED) transition is allowed according to the selection rules [40]. In the studied Eu^{3+}-doped PGFs systems, it is clearly seen that this transition has a lower integral intensity than the intensity of the $^5D_0 \rightarrow {}^7F_2$ transition and slightly more intense than the $^5D_0 \rightarrow {}^7F_1$ transition. This result is similar to several previously reported PG systems [29,45–49]. On the other hand, the intensities of the emission bands increase significantly with increasing Eu^{3+} ions concentration up to 6 mol% of Eu_2O_3, while the peaks are at the same energy positions with a rather similar shape. Similar results were obtained for PGs doped with different concentrations of Eu^{3+} [36,50,51].

The characteristic PL bands of PGFs in the (65-x) P_2O_5–35CaO–xTb system (with x = 3, 5, and 6 mol%) recorded under 374 nm excitation are attributed to Tb^{3+} ions. Several emission bands are observed from the $^5D_3$ and $^5D_4$ excited states in the blue and green/red spectral zone

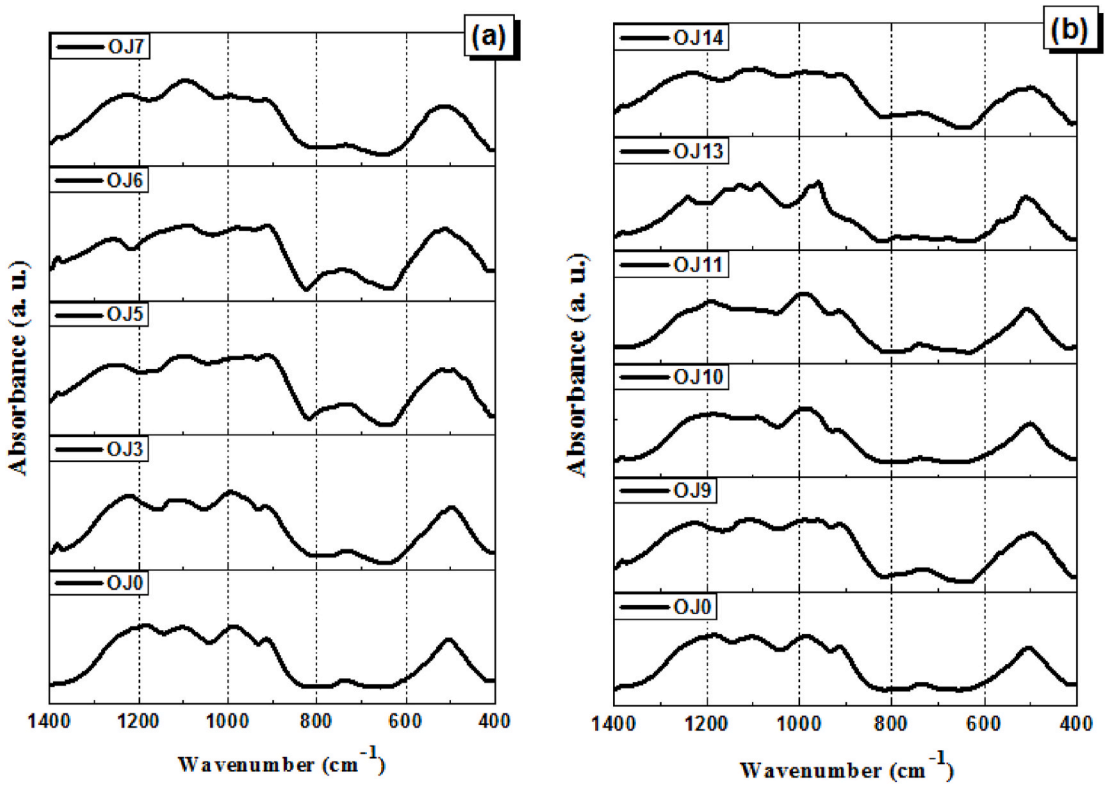

Fig. 6. FTIR spectra for the studied PGFs samples.

Table 4
Infrared band positions (cm^{-1}) and assignments of the PGFs samples.

Position (cm^{-1})	Assignment
~1231	Asymmetric stretching vibration $\upsilon_{as}(PO_2)$ (NBO* atoms; Q^2 species)
~1184	Symmetric stretching vibration $\upsilon_s(PO_2)$ (NBO* atoms; Q^2 species)
~1103	Asymmetric stretching vibration $\upsilon_{as}(PO_3)$ (NBO* atoms; Q^1 species)
~996	Symmetric stretching vibration $\upsilon_s(PO_3)$ (NBO* atoms; Q^1 species)
~915	Asymmetric stretching vibration υ_{as}(P—O—P) (BO* atoms; Q^2 species)
~741	Symmetric stretching vibration υ_s(P—O—P) (BO* atoms; Q^2 species)
~514	Bending vibration of $\delta(PO_4)^{3-}$ groups

*BO: bridging oxygen; *NBO: non bridging oxygen.

[30,52]. The bands from the $^5D_3$ level are located around 412 and 418, 433, 460, and 476 correspond to the emission transitions $^5D_3 \rightarrow {}^7F_5$, $^5D_3 \rightarrow {}^7F_4$, $^5D_3 \rightarrow {}^7F_3$, and $^5D_3 \rightarrow {}^7F_2$, respectively. The bands from the $^5D_4$ level are located around 490, 543, 582, 619, 654, 668, and 679 nm correspond to the emission transitions $^5D_4 \rightarrow {}^7F_6$, $^5D_4 \rightarrow {}^7F_5$, $^5D_4 \rightarrow {}^7F_4$, $^5D_4 \rightarrow {}^7F_3$, $^5D_4 \rightarrow {}^7F_2$, $^5D_4 \rightarrow {}^7F_1$, and $^5D_4 \rightarrow {}^7F_0$, respectively. The most intense band with green emission is at 543 nm, arises from the Laporte-forbidden $^5D_4 \rightarrow {}^7F_5$ (ED) transition [30,53]. This transition is hypersensitive to the Tb^{3+} environment [13]. Additionally, in the PL spectrum of PGFs doped with 6 mol % of Tb_2O_3, this band is divided into two components due to the Stark division of energy levels [7]. The $^5D_4 \rightarrow {}^7F_6$ transition obeys the (MD) transition selection rule of $\Delta J = \pm 1$ [53, 54]. Besides, this transition is almost independent of the environment [13]. The PL spectra show gradual increases in the intensity of the $^5D_4$ level bands with the increment of Tb^{3+}, while the peaks are at the same energy positions. The bands observed in the PL spectra of the $^5D_3$ level are due to a low rate of non-radiative processes from $^5D_3$ level to $^5D_4$ level [55]. These transitions are quenched at a high Tb^{3+} content when

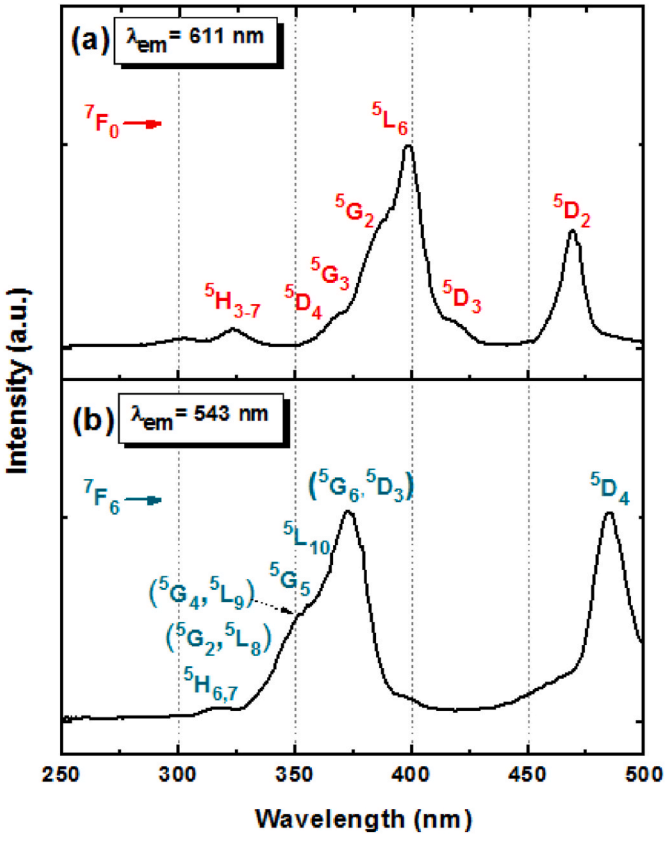

Fig. 7. Excitation spectra at 300K of **(a)** Eu^{3+}-doped PGFs for emission at 611 nm and **(b)** Tb^{3+}-doped PGFs for emission at 543 nm.

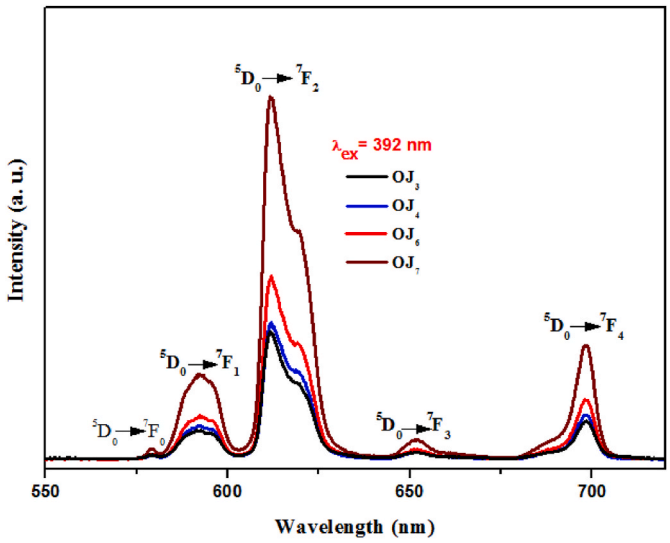

Fig. 8. Emission spectra of Eu^{3+}-doped PGFs samples under 392 nm excitation at 300 K.

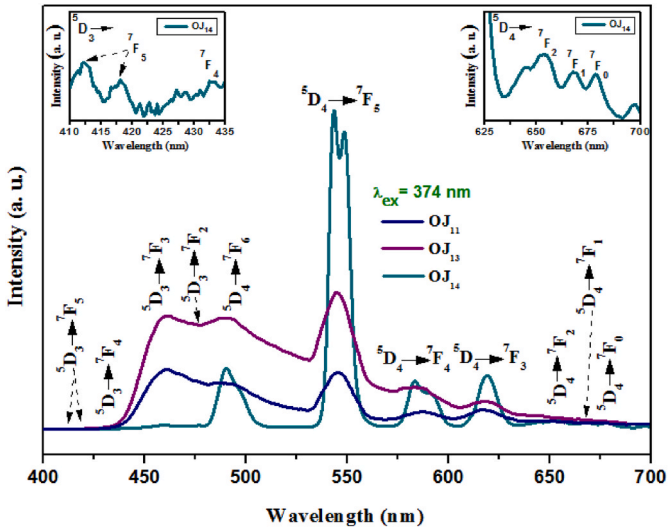

Fig. 9. Emission spectra of Tb^{3+}-doped PGFs samples under 374 nm excitation at 300 K.

the Tb_2O_3 content increased by 6 mol %. Previous works have indicated that the concentration of Tb^{3+} affects $^5D_3$ emission via the cross-relaxation (CR) process due to the reduction in distances [56–58]. Therefore, the band corresponding to the $^5D_3 \rightarrow {}^7F_3$ transition becomes too weak for the OJ_{14} sample.

The absolute quantum yield is described as the efficiency at which a material re-emits by fluorescence a certain number of photons absorbed at a given wavelength. Tables 5 and 6 show the calculated values of absolute quantum yield (Φa) for all PGFs samples in both series. It can be seen that Φa gradually increases with increasing Eu^{3+} or Tb^{3+} ions concentration. They vary from 3.61 to 20.25% for Eu^{3+}-doped fibers upon excitation at 392 nm, while for Tb^{3+}-doped fibers the Φa does not exceed 5% upon excitation at 374 nm. On the other hand, the internal quantum yield (Φi) varies by 62.80 ± 10.10% for OJ_7 PGFs and by 16.21 ± 4.85% for OJ_{14} PGFs, with *Abs* values increasing with RE^{3+} ions concentration. To the best of our knowledge, there are no internal or absolute quantum yield data available for glassy systems comparable to those studied in this paper. Therefore, the results reported in this work provide original reference data to compare various Eu^{3+} and Tb^{3+} doped luminescent glass materials.

Table 5
Calculated values of absolute quantum yields (Φa) for Eu^{3+}-doped PGFs samples.

PGFs	OJ_1	OJ_2	OJ_3	OJ_4	OJ_5	OJ_6	OJ_7
Φa (%)	3.61	8.84	12.47	16.75	17.32	18.31	20.25

Table 6
Calculated values of absolute quantum yields (Φa) for Tb^{3+}-doped PGFs samples.

PGFs	OJ_8	OJ_9	OJ_{10}	OJ_{11}	OJ_{12}	OJ_{13}	OJ_{14}
Φa (%)	0.59	1.57	1.99	2.24	2.63	3.78	4.81

At last, the CIE color coordinates emitted by the two PGFs samples OJ_7 and OJ_{14} are presented in the CIE 1931 chromaticity diagram in Fig. 10. OJ_7 fibers give average color coordinates (x = 0.648, y = 0.344) under 392 nm excitation and are found in the red light region. OJ_{14} fibers give average color coordinates (x = 0.295, y = 0.477) under 374 nm excitation and are situated in the green light region.

4. Conclusion

In this study, fifteen phosphate glasses (PGs) formulations were developed by the melt-quenching technique and divided into two glass systems (65-x) P_2O_5–35CaO–xEu_2O_3 and (65-x) P_2O_5–35CaO–xTb_2O_3, with $0 \leq x \leq 6$ mol%. All compositions were successfully drawn as continuous monofilaments phosphate glass fibers (PGFs). The average diameter was 22.1 ± 0.8 μm with a fixed spinning speed. Morphological analysis performed by SEM showed that the elaborated fibers have a homogeneous and smooth surface. Their amorphous nature was confirmed by XRD and DTA. The mechanical properties of undoped PGFs were higher than those of PGFs in the literature. A significant increase in mechanical quantities was noticed with the addition of 6 mol% of RE_2O_3 (RE = Eu or Tb). The values of tensile strength, Young's modulus, and breaking strain were 1031 ± 34 MPa, 80 ± 6 GPa, and 1.29 ± 0.23%, respectively, for fibers doped with 6 mol% of Eu_2O_3 (OJ_7), and 1014 ± 65 MPa, 79 ± 7 GPa, and 1.28 ± 0.20%, respectively,

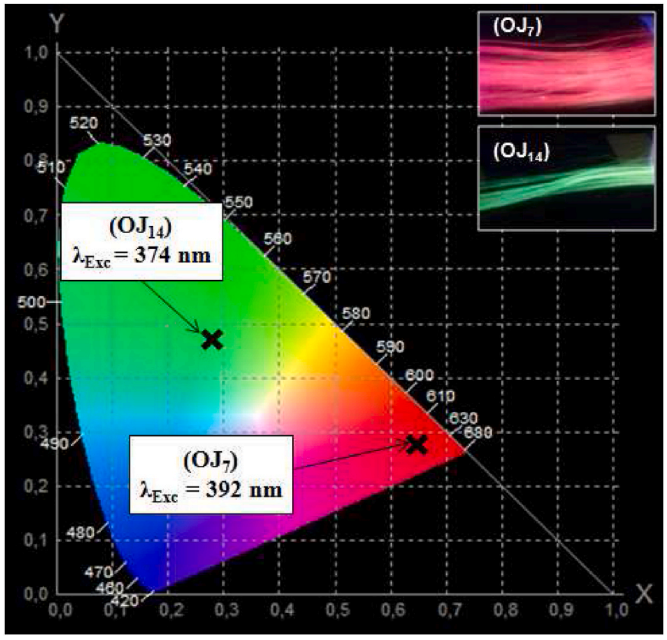

Fig. 10. CIE color coordinates of PGFs samples on CIE 1931 chromaticity diagram upon excitation at 392 nm (OJ_7) and 374 nm (OJ_{14}).

for fibers doped with 6 mol% of Tb_2O_3 (OJ_{14}). The strong aggregation of Eu^{3+} and Tb^{3+} ions that occupy the interstitial sites of the glassy network increased the density with a simultaneous decrease of the molar volume, making the glassy network more compact. Thus, the Tg was also increased with increasing RE_2O_3 content. The undoped and doped fibers up to 5 mol% of RE_2O_3 belong to the ultraphosphate groups rich in (Q^3). When O/P = 3 for fibers doped with 6 mol% of RE_2O_3, the meta-phosphate groups rich in (Q^2) become dominant. This result indicates that the bond length and bond angle of P–O–P in the glassy network structure also change. However, no significant changes are observed in the FTIR spectra. The photoluminescence properties of PGFs doped with different RE_2O_3 contents were discussed in detail. The most intense emission band at 611 nm corresponds to the $^5D_0 \rightarrow {}^7F_2$ transition, leads to the red emission with a maximum absolute quantum yield equal to 20.25% observed for the OJ_7 sample. The most intense emission band at 543 nm corresponds to the $^5D_4 \rightarrow {}^7F_5$ transition, leads to the green emission with a maximum absolute quantum yield equal to about 5% for the OJ_{14} sample. The CIE color coordinates for these two compositions were found to (x = 0.648, y = 0.344) and (x = 0.295, y = 0.477) lying in the red and green regions, respectively.

Given all that, we have therefore demonstrated that it is possible to synthesize PGFs with excellent luminescent properties and that the doping of Eu^{3+} and Tb^{3+} ions in the studied glass systems improves the mechanical performance and influences the structural properties of the investigated PGFs.

Declaration of competing interest

The authors declare that they have no known competing financial interests or personal relationships that could have appeared to influence the work reported in this paper.

Acknowledges

This work was supported financially by grants from the PHC-Toubkal under the project TBK/15/16, Campus France: 32506VM. We also thank the Higher School of Textiles and Clothing Industries (ESITH) and the Faculty of Sciences Ben M'scik (FSBM) for their continued support of this work.

References

[1] O. Jamal Eddine, et al., Elaboration and characterization of new phosphate glasses based on natural phosphate and red clay: influence of the chemical composition on the chemical durability, Mediterr. J. Chem. 9 (3) (2019) 222–235, https://doi.org/10.13171/mjc93191012614sg.

[2] A.A. Reddy, et al., Optical properties of Dy^{3+}-doped sodium–aluminum–phosphate glasses, J. Mater. Sci. 46 (7) (2011) 2018–2023, https://doi.org/10.1007/s10853-010-4851-3.

[3] V. Venkatramu, et al., Optical spectroscopy of Sm^{3+} ions in phosphate and fluorophosphate glasses, Opt. Mater. 29 (11) (2007) 1429–1439, https://doi.org/10.1016/j.optmat.2006.06.011.

[4] I.A.M. Ibrahim, et al., Electronic structure and energy level schemes of RE^{3+}: $LaSi_3N_5$ and RE^{2+}: $LaSi_3N_{5-x}O_x$ phosphors (RE= Ce, Pr, ND, Pm, Sm, Eu) from first principles, J. Lumin. 164 (2015) 131–137, https://doi.org/10.1016/j.jlumin.2015.03.035.

[5] L. Han, et al., A novel Eu^{3+}-doped phosphate glass for reddish orange emission: preparation, structure and fluorescence properties, J. Lumin. 221 (2020) 117041, https://doi.org/10.1016/j.jlumin.2020.117041.

[6] R.M. Zaki, et al., Direct 3D-printing of phosphate glass by fused deposition modeling, Mater. Des. 194 (2020) 108957, https://doi.org/10.1016/j.matdes.2020.108957.

[7] L. Zhang, et al., An investigation of the optical properties of Tb^{3+}-doped phosphate glasses for green fiber laser, Opt. Mater. 34 (7) (2012) 1202–1207, https://doi.org/10.1016/j.optmat.2012.01.031.

[8] S. Rada, E. Culea, FTIR spectroscopic and DFT theoretical study on structure of europium–phosphate–tellurate glasses and glass ceramics, J. Mol. Struct. 929 (1–3) (2009) 141–148, https://doi.org/10.1016/j.molstruc.2009.04.021.

[9] H. Ebendorff-Heideprie, D. Ehrt, Relationships between glass structure and spectroscopic properties of Eu^{3+} and Tb^{3+} doped glasses, Ber. Bunsenges. Physik. Chem. 100 (9) (1996) 1621–1624, https://doi.org/10.1002/bbpc.19961000955.

[10] C.R. Kesavulu, et al., Concentration effect on the spectroscopic behavior of Tb^{3+} ions in zinc phosphate glasses, J. Lumin. 165 (2015) 77–84, https://doi.org/10.1016/j.jlumin.2015.04.012.

[11] C.M. Reddy, et al., A review on optical and photoluminescence studies of RE^{3+} (RE= Sm, Dy, Eu, Tb and Nd) ions doped LCZSFB glasses, Renew. Sustain. Energy Rev. 51 (2015) 566–584, https://doi.org/10.1016/j.rser.2015.06.025.

[12] K. Binnemans, Interpretation of europium (III) spectra, Coord. Chem. Rev. 295 (2015) 1–45, https://doi.org/10.1016/j.ccr.2015.02.015.

[13] Y. Chen, et al., Photoluminescence of Tb-doped MgAl-LDHs depending on phase transition caused by annealing, J. Rare Earths 34 (1) (2016) 36–44, https://doi.org/10.1016/S1002-0721(14)60575-5.

[14] P. Avouris, A. Campion, M.A. El-Sayed, Phonon assisted site-to-site electronic energy transfer between Eu^{3+} ions in an amorphous solid, Chem. Phys. Lett. 50 (1) (1977) 9–13, https://doi.org/10.1016/0009-2614(77)80669-6.

[15] E. Nakazawa, S. Shionoya, Relaxation between excited levels of Tb^{3+} ion due to resonance energy transfer, J. Phys. Soc. Japan 28 (5) (1970) 1260–1265, https://doi.org/10.1143/JPSJ.28.1260.

[16] E. Takushi, T. Kushida, Anomalous spectral properties of inhomogeneously broaded transitions of Eu^{3+} in $Ca(PO_3)_2$ glass, J. Lumin. 18 (1979) 661–664, https://doi.org/10.1016/0022-2313(79)90213-8.

[17] J.R. Morgan, M.A. El-Sayed, Temporal and temperature dependence of the energy transfer process among europium (3+) in an amorphous solid, J. Phys. Chem. 85 (24) (1981) 3566–3568, https://doi.org/10.1021/j150624a008.

[18] G. Nishimura, et al., $^5D_0$-$^7F_0$ transition mechanism of Eu^{3+} in $Ca(PO_3)_2$ glass, Y_2O_2S crystal and polyvinyl alcohol, J. Lumin. 48 (1991) 473–476, https://doi.org/10.1016/0022-2313(91)90172-R.

[19] D. Bricis, et al., Magnetic circular dichroism of the optical absorption and optically detected ESR of X-irradiated Tb^{3+} doped and undoped $CaO \cdot P_2O_5$ glasses, Solid State Commun. 81 (9) (1992) 745–748, https://doi.org/10.1016/0038-1098(92)90781-4.

[20] O. Jamal Eddine, et al., Effect of the chemical composition on the structural and mechanical properties of phosphate glass fibers based on natural phosphate, J. Alloys Compd. 817 (2020) 152808, https://doi.org/10.1016/j.jallcom.2019.152808.

[21] O. Jamal Eddine, et al., Mechanical, structural, and chemical properties of unmodified and iron-modified phosphate glass fibers based on natural phosphate and kaolin clay, Mater. Chem. Phys. 255 (2020) 123573, https://doi.org/10.1016/j.matchemphys.2020.123573.

[22] Carbon fibre – determination of the tensile properties of single filament specimens, international standard, ISO 11566, BS ISO 11566 (1996).

[23] M.A. Slivka, C.C. Chu, I.A. Adisaputro, Fiber-matrix interface studies on bioabsorbable composite materials for internal fixation of bone fractures. I. Raw material evaluation and measurement of fiber—matrix interfacial adhesion, J. Biomed. Mater. Res. 36 (4) (1997) 469–477, https://doi.org/10.1002/(SICI)1097-4636(19970915)36:4<469::AID-JBM4>3.0.CO;2-C.

[24] I. Ahmed, et al., Weight loss, ion release and initial mechanical properties of a binary calcium phosphate glass fibre/PCL composite, Acta Biomater. 4 (5) (2008) 1307–1314, https://doi.org/10.1016/j.actbio.2008.03.018.

[25] R.K. Brow, et al., The effects of melt history on the failure characteristics of pristine glass fibres, Phys. Chem. Glasses 50 (1) (2009) 31–33.

[26] R.O. Omrani, et al., Structural and thermochemical study of Na_2O–ZnO–P_2O_5 glasses, J. Non-Cryst. Solids 390 (2014) 5–12, https://doi.org/10.1016/j.jnoncrysol.2014.02.020.

[27] A.M.B. Silva, et al., Structural characterization of TiO_2–P_2O_5–CaO glasses by spectroscopy, J. Eur. Ceram. Soc. 30 (6) (2010) 1253–1258, https://doi.org/10.1016/j.jeurceramsoc.2009.11.001.

[28] G. El-Damrawi, A.K. Hassan, A. Shahboub, ^{31}P and ^{27}Al nuclear magnetic resonance studies on silver phosphate glasses, Magn. Reson. Solids 20 (2) (2018).

[29] M. Elisa, et al., Optical and structural characterization of samarium and europium-doped phosphate glasses, J. Non-Cryst. 369 (2013) 55–60, https://doi.org/10.1016/j.jnoncrysol.2013.03.024.

[30] S. Sharma, S. Jana, Luminescence properties of Tb^{3+} embedded zinc lead phosphate glasses, Mater. Chem. Phys. 251 (2020) 122968, https://doi.org/10.1016/j.matchemphys.2020.122968.

[31] S.M. Abo-Naf, et al., In vitro bioactivity evaluation, mechanical properties and microstructural characterization of Na_2O–CaO–B_2O_3–P_2O_5 glasses, Spectrochim, Acta A Mol. Biomol. Spectrosc. 144 (2015) 88–98, https://doi.org/10.1016/j.saa.2015.02.076.

[32] W. Jastrzębski, et al., Infrared spectroscopy of different phosphates structures, Spectrochim. Acta Mol. Biomol. Spectrosc. 79 (4) (2011) 722–727, https://doi.org/10.1016/j.saa.2010.08.044.

[33] H.R.A. Mooghari, et al., The effects of SiO_2 and K_2O on glass forming ability and structure of $CaOTiO_2P_2O_5$ glass system, Ceram. Int. 38 (4) (2012) 3281–3290, https://doi.org/10.1016/j.ceramint.2011.12.034.

[34] R. Reisfeld, Spectra and energy transfer of rare earths in inorganic glasses, in: Rare Earths, vol. 13, Springer, Berlin, Heidelberg, 1973, pp. 53–98, https://doi.org/10.1007/3-540-06125-8_2.

[35] B. Padlyak, A. Drzewiecki, Spectroscopy of the CaB_4O_7 and $LiCaBO_3$ glasses, doped with terbium and dysprosium, J. Non-Cryst. 367 (2013) 58–69, https://doi.org/10.1016/j.jnoncrysol.2013.02.018.

[36] K. Linganna, C.K. Jayasankar, Optical properties of Eu^{3+} ions in phosphate glasses, Spectrochim. Acta Mol. Biomol. Spectrosc. 97 (2012) 788–797, https://doi.org/10.1016/j.saa.2012.07.031.

[37] A.K. Parchur, R.S. Ningthoujam, Behaviour of electric and magnetic dipole transitions of Eu^{3+}, $^5D_0 \rightarrow {}^7F_0$ and Eu–O charge transfer band in Li^+ co-doped YPO_4: Eu^{3+}, RSC Adv. 2 (29) (2012) 10859–10868, https://doi.org/10.1039/c2ra22144f.

[38] P. Porcher, P. Caro, Influence of J-mixing on the phenomenological interpretation of the Eu^{3+} ion spectroscopic properties, J. Lumin. 21 (2) (1980) 207–216, https://doi.org/10.1016/0022-2313(80)90022-8.
[39] M. Tanaka, G. Nishimura, T. Kushida, Contribution of J mixing to the $^5D_0 - {}^7F_0$ transition of Eu^{3+} ions in several host matrices, Phys. Rev. B 49 (24) (1994) 16917, https://doi.org/10.1103/PhysRevB.49.16917.
[40] I.I. Kindrat, et al., Enhancement of the Eu^{3+} luminescence in $Li_2B_4O_7$ glasses co-doped with Eu and Ag, J. Lumin. 204 (2018) 122–129, https://doi.org/10.1016/j.jlumin.2018.07.051.
[41] H. Wen, et al., Understanding Eu^{3+} emission spectra in glass, Phys. Chem. Chem. Phys. 12 (33) (2010) 9933–9937, https://doi.org/10.1039/C0CP00206B.
[42] J. Pisarska, et al., Local structure and luminescent properties of lead phosphate glasses containing rare earth ions, J. Rare Earths 29 (12) (2011) 1157–1160, https://doi.org/10.1016/S1002-0721(10)60616-3.
[43] C. Görller-Walrand, et al., Magnetic dipole transitions as standards for Judd–Ofelt parametrization in lanthanide spectra, J. Chem. Phys. 95 (5) (1991) 3099–3106, https://doi.org/10.1063/1.460867.
[44] J.E. Lowther, Spectroscopic transition probabilities of rare earth ions, J. Phys. C Solid State Phys. 7 (23) (1974) 4393, https://doi.org/10.1088/0022-3719/7/23/026.
[45] R. Balakrishnaiah, et al., Characterization of Eu^{3+}-doped fluorophosphate glasses for red emission, J. Non-Cryst. 353 (13–15) (2007) 1397–1401, https://doi.org/10.1016/j.jnoncrysol.2006.10.063.
[46] S.S. Babu, et al., Optical absorption and photoluminescence studies of Eu^{3+}-doped phosphate and fluorophosphate glasses, J. Lumin. 126 (1) (2007) 109–120, https://doi.org/10.1016/j.jlumin.2006.05.010.
[47] H. Ebendorff-Heidepriem, D. Ehrt, Spectroscopic properties of Eu^{3+} and Tb^{3+} ions for local structure investigations of fluoride phosphate and phosphate glasses, J. Non-Cryst. 208 (3) (1996) 205–216, https://doi.org/10.1016/S0022-3093(96)00524-8.
[48] Y. Chen, et al., Down-conversion luminescence and optical thermometric performance of Tb^{3+}/Eu^{3+} doped phosphate glass, J. Non-Cryst. 484 (2018) 111–117, https://doi.org/10.1016/j.jnoncrysol.2018.01.027.
[49] L.M. Marcondes, et al., High tantalum oxide content in Eu^{3+}-doped phosphate glass and glass-ceramics for photonic applications, J. Alloys Compd. 842 (2020) 155853, https://doi.org/10.1016/j.jallcom.2020.155853.
[50] R. Priyanka, et al., Structural and spectroscopic investigations on Eu^{3+} ions doped boro-phosphate glasses for optical display applications, J. Lumin. 220 (2020) 116964, https://doi.org/10.1016/j.jlumin.2019.116964.
[51] P. Aryal, et al., Development of Eu^{3+}-doped phosphate glass for red luminescent solid-state optical devices, J. Lumin. 227 (2020) 117564, https://doi.org/10.1016/j.jlumin.2020.117564.
[52] Z. Liu, Rare Earths: New Research, Nova Science Publishers, New York, 2013.
[53] P.A. Azeem, et al., Spectroscopic investigations on Tb^{3+} doped lead fluoroborate glasses, Opt Commun. 285 (18) (2012) 3787–3791, https://doi.org/10.1016/j.optcom.2012.05.034.
[54] M. Venkateswarlu, B.H. Rudramadevi, Luminescence analysis of Eu^{3+} and Tb^{3+} ions doped borate zinc magnesium glasses, Int. J. Sci. Res. 4 (4) (2015) 3179–3184.
[55] V.X. Quang, et al., Role of modifier ion radius in luminescence enhancement from $^5D_4$ level of Tb^{3+} ion doped alkali-alumino-telluroborate glasses, J. Lumin. 221 (2020) 117039, https://doi.org/10.1016/j.jlumin.2020.117039.
[56] A.U. Trápala-Ramírez, et al., Calcium-zinc phosphate glasses activated with Tb^{3+}/Eu^{3+} for laser and white LED applications, J. Lumin. 215 (2019) 116621, https://doi.org/10.1016/j.jlumin.2019.116621.
[57] H.I. Francisco-Rodriguez, et al., Lithium-aluminum-zinc phosphate glasses activated with Tb^{3+} and Tb^{3+}/Eu^{3+} for green laser medium, reddish-orange and white phosphor applications, Opt. Mater. 79 (2018) 358–365, https://doi.org/10.1016/j.optmat.2018.04.004.
[58] R. Martínez-Martínez, et al., Cold white light generation from hafnium oxide films activated with Ce^{3+}, Tb^{3+}, and Mn^{2+} ions, J. Mater. Res. 25 (3) (2010) 484–490, https://doi.org/10.1557/JMR.2010.0065.